

# High-temperature tribological properties of Al<sub>2</sub>O<sub>3</sub>, Ni–20 mass% Cr and NiAl spark-plasma-sintered composites containing BaF<sub>2</sub>–CaF<sub>2</sub> phase

T. Murakami<sup>a,\*</sup>, J.H. Ouyang<sup>a</sup>, S. Sasaki<sup>a</sup>, K. Umeda<sup>a</sup>, Y. Yoneyama<sup>b</sup>

<sup>a</sup> National Institute of Advanced Industrial Science and Technology, Tsukuba, Japan

<sup>b</sup> Tokyo University of Science, Noda, Chiba, Japan

Received 2 August 2004; received in revised form 22 December 2004; accepted 24 December 2004

Available online 20 January 2005

## Abstract

Al<sub>2</sub>O<sub>3</sub>, Ni–20 mass% Cr, NiAl-based composites containing BaF<sub>2</sub>, CaF<sub>2</sub> and SrF<sub>2</sub> as solid lubricants were prepared by spark plasma sintering, and their microstructure and high-temperature friction and wear properties were examined. Al<sub>2</sub>O<sub>3</sub>–31BaF<sub>2</sub>–19CaF<sub>2</sub> (mass%) composites prepared by spark plasma sintering at 1273 K contained a fine lamellar structure, which consisted of BaF<sub>2</sub> and CaF<sub>2</sub> phases. The Al<sub>2</sub>O<sub>3</sub>–31BaF<sub>2</sub>–19CaF<sub>2</sub> (mass%) composites showed a low friction coefficient (0.3–0.4) at temperatures between room temperature and 1073 K, in addition that they showed the lowest wear rate at 873 K. In this study, a tentative BaF<sub>2</sub>–CaF<sub>2</sub>–SrF<sub>2</sub> ternary phase diagram was also constructed, which clarified that the BaF<sub>2</sub>–CaF<sub>2</sub>–SrF<sub>2</sub> ternary system has a large solid solution region at 1473 K.  
© 2004 Elsevier B.V. All rights reserved.

**Keywords:** Self-lubricating composites; Spark plasma sintering; NiAl; CaF<sub>2</sub>; BaF<sub>2</sub>

## 1. Introduction

Nickel alloys and ceramics containing solid lubricants have attracted much attention as high-temperature self-lubricating materials [1–9]. In particular, Sliney et al. reported that Ni–Cr alloys containing fluorides such as BaF<sub>2</sub>–CaF<sub>2</sub> eutectic (BaF<sub>2</sub>–38 mass% CaF<sub>2</sub>) exhibited low friction at high temperatures [1,2]. However, the oxidation resistance of the composite films was insufficient at high temperatures. Replacing the Ni–Cr alloy phases in the composites with Al<sub>2</sub>O<sub>3</sub> and NiAl phases, which show much better oxidation resistance than the Ni–Cr alloys, may improve their oxidation resistance. On the other hand, some compositions in the BaF<sub>2</sub>–CaF<sub>2</sub>–SrF<sub>2</sub> system may exhibit lower friction than BaF<sub>2</sub>–CaF<sub>2</sub> eutectic, because SrF<sub>2</sub> has the same crystal structure as CaF<sub>2</sub> and BaF<sub>2</sub>. However, the

BaF<sub>2</sub>–CaF<sub>2</sub>–SrF<sub>2</sub> ternary phase diagram has not been reported clearly, and the friction and wear properties of composites containing SrF<sub>2</sub> have not been clarified. In this study, Al<sub>2</sub>O<sub>3</sub>, Ni–20 mass% Cr and NiAl composites containing BaF<sub>2</sub> and CaF<sub>2</sub>, which had the same composition as the BaF<sub>2</sub>–CaF<sub>2</sub> eutectic, were prepared using spark plasma sintering (SPS), and their friction and wear properties against a Al<sub>2</sub>O<sub>3</sub> ball in air were investigated at temperatures between room temperature and 1073 K. SPS is a method of preparing alloy-based and ceramic-based composites for a short sintering time easily [9–15], and the sintering is carried out by flowing pulse dc current through the graphite mold, in which sample powders are set. In addition, the high-temperature friction and wear properties of Al<sub>2</sub>O<sub>3</sub>-based composites containing CaF<sub>2</sub> and SrF<sub>2</sub> were also examined. Moreover, a tentative BaF<sub>2</sub>–CaF<sub>2</sub>–SrF<sub>2</sub> ternary phase diagram was constructed by investigating X-ray diffraction patterns and the microstructure of spark-plasma-sintered specimens of this system.

\* Corresponding author. Tel.: +81 29861 7190; fax: +81 29861 7844.  
E-mail address: [murakami.t@aist.go.jp](mailto:murakami.t@aist.go.jp) (T. Murakami).

Table 1

Compositions and spark plasma sintering conditions of Al<sub>2</sub>O<sub>3</sub>, Ni–20 mass% Cr and NiAl-based composites investigated in this study

Sample ID	Composition (mass%)	Sintering temperature (K)	Sintering pressure (MPa)	Sintering time (ks)	Relative density (%)
1A	Al <sub>2</sub> O <sub>3</sub> –31BaF <sub>2</sub> –19CaF <sub>2</sub>	1273	40	0.6	97.5
1B	Al <sub>2</sub> O <sub>3</sub> –31BaF <sub>2</sub> –19CaF <sub>2</sub> –5SiO <sub>2</sub>	1123	40	1.2	94.9
1C	Ni–10Cr–31BaF <sub>2</sub> –19CaF <sub>2</sub>	1123	40	0.3	98.5
1D	NiAl–31BaF <sub>2</sub> –19CaF <sub>2</sub>	1123	40	0.3	97.5
1E	Al <sub>2</sub> O <sub>3</sub> –50CaF <sub>2</sub>	1523	40	0.6	97.2
1F	Al <sub>2</sub> O <sub>3</sub> –50SrF <sub>2</sub>	1523	40	0.6	98.8

## 2. Experimental procedures

Compositions of the Al<sub>2</sub>O<sub>3</sub>, Ni–20 mass% Cr and NiAl-based composites investigated in this study are shown in Table 1. The composite with a composition of Al<sub>2</sub>O<sub>3</sub>–31BaF<sub>2</sub>–19CaF<sub>2</sub> (mass%) consists of 50 mass% Al<sub>2</sub>O<sub>3</sub> and 50 mass% fluorides whose composition is the same as BaF<sub>2</sub>–CaF<sub>2</sub> eutectic (BaF<sub>2</sub>–38 mass% CaF<sub>2</sub>). The composites of 20 mm in diameter and 5 mm in thickness as shown in Table 1 were prepared by blending the powders shown in Table 2 using a hexane-filled ball mill, and spark plasma sintering the blended powders in the conditions shown in Table 1. Temperature was measured at the surface of graphite mold during sintering. In this paper, the Al<sub>2</sub>O<sub>3</sub>–31BaF<sub>2</sub>–19CaF<sub>2</sub>, Al<sub>2</sub>O<sub>3</sub>–31BaF<sub>2</sub>–19CaF<sub>2</sub>–5SiO<sub>2</sub>, Ni–10Cr–31BaF<sub>2</sub>–19CaF<sub>2</sub>, NiAl–31BaF<sub>2</sub>–19CaF<sub>2</sub>, Al<sub>2</sub>O<sub>3</sub>–50CaF<sub>2</sub> and Al<sub>2</sub>O<sub>3</sub>–50SrF<sub>2</sub> (mass%) composites are referred to as the specimens 1A, 1B, 1C, 1D, 1E and 1F, respectively. After the sintering, X-ray diffraction pattern, relative density, microvickers hardness and microstructure of each composite were examined. In addition, the friction and wear properties of each composite were investigated using a reciprocating ball-on-disk tribometer [6,7] against Al<sub>2</sub>O<sub>3</sub> balls (9.53 mm in diameter) at temperatures between room temperature and 1073 K in static room air of relative humidity ranging from 60 to 70%. Before the friction tests, each specimen was polished using 4000 grit emery papers and cleaned in the mixture of 50 vol% acetone and 50 vol% petroleum benzene for 0.6 ks using an ultrasonic cleaner. The surface roughness, hardness and density of the Al<sub>2</sub>O<sub>3</sub> balls used in the friction tests were 0.02 μm R<sub>a</sub>, 16.5 GPa and 3.95 Mg/m<sup>3</sup>, respectively, while the surface roughness of specimens 1A, 1C–F was 5.6 × 10<sup>−2</sup>, 3.1 × 10<sup>−1</sup>, 2.7, 9.1 × 10<sup>−1</sup> and 1.9 × 10<sup>−1</sup> μm R<sub>a</sub>, respectively. The reason why each specimen showed different surface roughness

Table 2

Properties of Al<sub>2</sub>O<sub>3</sub>, Ni–20 mass% Cr, NiAl, SiO<sub>2</sub>, BaF<sub>2</sub>, CaF<sub>2</sub> and SrF<sub>2</sub> powders used in this study

Powder ID	Composition	Properties
a	Al <sub>2</sub> O <sub>3</sub>	99.99% pure, 0.1 μm
b	Ni–20 mass% Cr	5–25 μm
c	NiAl	99.5% pure, −100 mesh
d	SiO <sub>2</sub>	99.99% pure, 2 μm
e	BaF <sub>2</sub>	95% pure, −45 μm
f	CaF <sub>2</sub>	10–45 μm
g	SrF <sub>2</sub>	99.5% pure, −45 μm

would be that each specimen had different grain size, relative density and hardness from the other specimens. In the friction tests, the operations to heat each specimen at the rate of 0.83 K/s to 473 K after measuring its friction coefficient for 1.2 ks at room temperature, hold the specimen at 473 K for 0.3 ks and measure for 1.2 ks were carried out to 1073 K. Also, the operations to heat each specimen at the rate of 0.83 K/s from room temperature to 873 K and measure its friction coefficient at 873 K for 3.6 ks were carried out. The testing conditions were 4.9 N load, 1 Hz frequency and 10 mm stroke. The friction coefficient was calculated by measuring the friction force at 1 ms intervals, obtaining the average friction force (absolute value) of one cycle of the reciprocation (1 s) and dividing the average friction force by load. In addition, the average friction coefficient of each specimen was calculated by averaging the friction coefficients in the time range of 60 s after starting the friction testing to the finishing time of the testing. After the testing, the wear rates and microstructure of the wear track of each specimen were investigated using a surface profilometer and a scanning electron microscope (SEM) with an energy dispersive spectroscopy (EDS) attachment, respectively. The high-temperature microvickers hardness of spark-plasma-sintered CaF<sub>2</sub>, SrF<sub>2</sub> and BaF<sub>2</sub>–38 mass% CaF<sub>2</sub> specimens was also investigated.

The compositions investigated for the construction of the BaF<sub>2</sub>–CaF<sub>2</sub>–SrF<sub>2</sub> ternary phase diagram are shown in Table 3. The mixture of powders e, f and g with the compositions shown in Table 3 were spark-plasma-sintered in the conditions of Table 3, and annealed at 1473 K for 86.4 ks in an Ar gas atmosphere. Before and after the heat treatment, X-ray

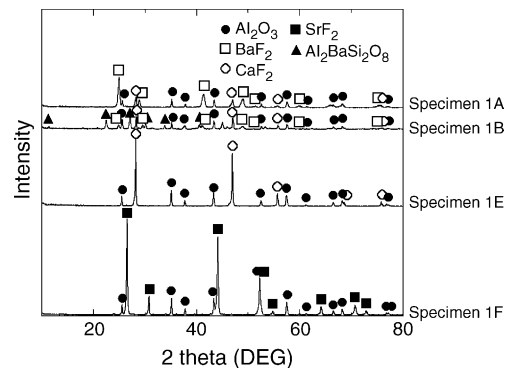


Fig. 1. X-ray diffraction patterns of specimens 1A, 1B, 1E and 1F.

Table 3

Compositions and spark plasma sintering conditions of specimens investigated for the construction of the BaF<sub>2</sub>–CaF<sub>2</sub>–SrF<sub>2</sub> ternary phase diagram

Specimen ID	Composition (mass%)	Sintering temperature (K)	Sintering pressure (MPa)	Sintering time (ks)
2A	BaF <sub>2</sub> –38CaF <sub>2</sub> <sup>a</sup>	1123	40	0.3
2B	BaF <sub>2</sub> –20SrF <sub>2</sub>	1373	40	0.3
2C	BaF <sub>2</sub> –50SrF <sub>2</sub>	1373	40	0.3
2D	CaF <sub>2</sub> –50SrF <sub>2</sub>	1573	40	0.3
2E	CaF <sub>2</sub> –70SrF <sub>2</sub>	1573	40	0.3
2F	BaF <sub>2</sub> –33.3CaF <sub>2</sub> –33.3SrF <sub>2</sub>	1323	40	0.3
2G	BaF <sub>2</sub> –20CaF <sub>2</sub> –60SrF <sub>2</sub>	1473	40	0.3

<sup>a</sup> Eutectic composition.

diffraction patterns and the microstructure of each specimen were examined.

### 3. Results and discussion

#### 3.1. High-temperature friction and wear properties of Al<sub>2</sub>O<sub>3</sub>, NiAl and Ni–20 mass% Cr-based composites

Fig. 1 shows X-ray diffraction patterns of spark-plasma-sintered Al<sub>2</sub>O<sub>3</sub>-based composites containing BaF<sub>2</sub>, CaF<sub>2</sub> and SrF<sub>2</sub>. No reaction product phases were observed in the specimens 1A, E and F, although Al<sub>2</sub>BaSi<sub>2</sub>O<sub>8</sub> phase was observed in the specimen 1B which contained 5 mass%

SiO<sub>2</sub> as a sintering additive. When SiO<sub>2</sub> was added to Al<sub>2</sub>O<sub>3</sub>–BaCrO<sub>4</sub> composites, no reaction product phases were observed in our previous study [9]. In addition, it was clarified in our previous study that the hardness and wear resistance of Al<sub>2</sub>O<sub>3</sub>–BaCrO<sub>4</sub> composites containing SiO<sub>2</sub> was much higher than those without sintering additives [9]. However, adding SiO<sub>2</sub> to Al<sub>2</sub>O<sub>3</sub>–31BaF<sub>2</sub>–19CaF<sub>2</sub> (mass%) composites reduced the volume fraction of BaF<sub>2</sub> phase, which indicates that their friction and wear properties are expected to worsen. No reaction product phases were observed in specimens 1C and 1D similarly to the specimen 1A.

Fig. 2 shows cross sections of specimens 1A, 1C, 1D, 1E, 1F. A fine lamellar structure was observed in the specimen 1A, while no lamellar structure was formed in the other

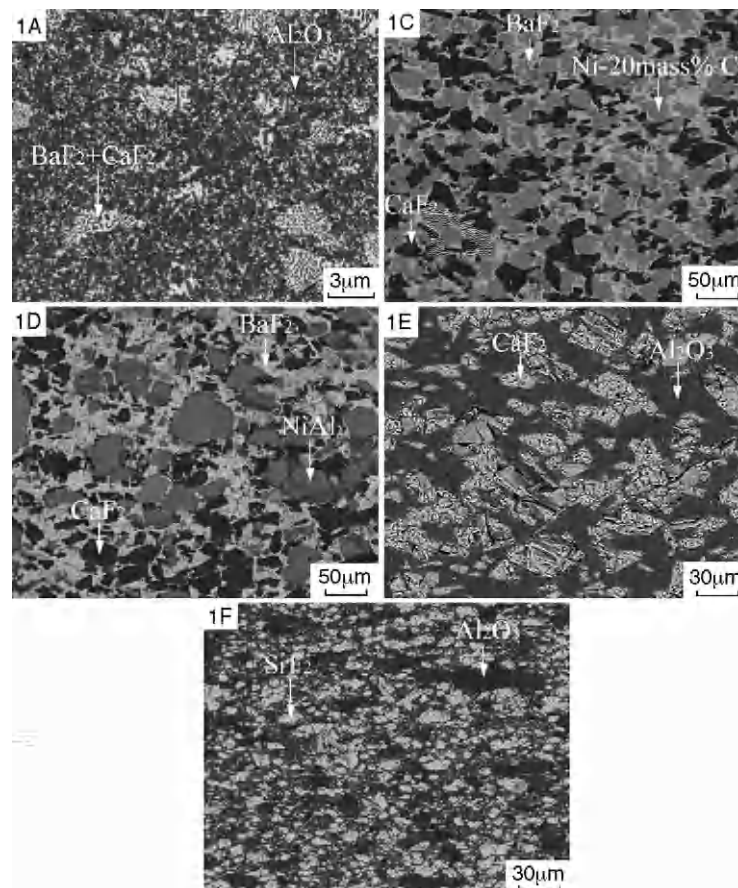


Fig. 2. SEM photographs showing cross sections of specimens 1A, 1C, 1D, 1E and 1F.

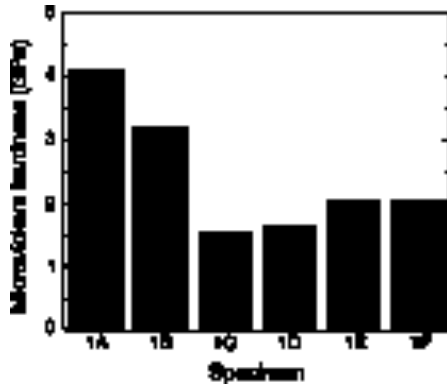


Fig. 3. Microvickers hardness of each specimen at room temperature. All the hardness was measured with a load of 9.8 N.

specimens. According to the EDS analysis, this lamellar microstructure consisted of BaF<sub>2</sub> and CaF<sub>2</sub> phases. It is reported that the eutectic temperature of the BaF<sub>2</sub>–CaF<sub>2</sub> system is 1295 K [16]. In addition, the temperature of specimen is normally 50–100 K higher than that at the surface of the graphite mold during SPS [15]. When the specimen 1A was prepared by sintering at 1273 K, which was the temperature at the surface of the mold, the temperature at the specimen might have exceeded the eutectic temperature. Therefore, BaF<sub>2</sub> and CaF<sub>2</sub> phases were melted during the SPS, and the lamellar structure would have formed during the cooling.

Fig. 3 shows the microvickers hardness of each specimen at room temperature. The microvickers hardness of specimen 1A was higher than those of the other Al<sub>2</sub>O<sub>3</sub>-based composites (specimens 1E and 1F). The reason would be that the specimen 1A had much finer microstructure than specimens 1E and 1F as shown in Fig. 2. In addition, it was clarified that the microvickers hardness of specimen 1A was reduced by adding SiO<sub>2</sub>.

Fig. 4 shows the average friction coefficients of specimens 1A, 1C, 1D, 1E and 1F. The specimen 1A showed the lowest friction coefficient (0.3–0.4) in the temperature range of room temperature to 1073 K, while friction coefficients of specimens 1C and 1D were higher than 0.5 below 473 and

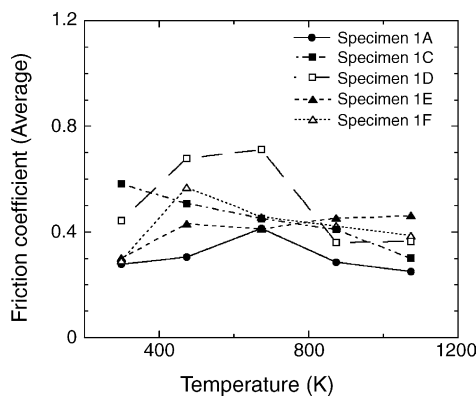


Fig. 4. Average friction coefficients of Al<sub>2</sub>O<sub>3</sub>, Ni–20mass% Cr and NiAl-based composites.

673 K, respectively. The high friction coefficients of specimens 1C and 1D would be obtained because Ni–Cr alloy and NiAl welded to the coupled Al<sub>2</sub>O<sub>3</sub> balls more easily than Al<sub>2</sub>O<sub>3</sub>. The friction coefficients of specimen 1E increased with increasing testing temperature, although it was reported that CaF<sub>2</sub> acted as a solid lubricant at temperatures between 673 and 1223 K [17]. As shown in Fig. 2, a lot of cracks were observed in the CaF<sub>2</sub> phase in specimen 1E. Therefore, the CaF<sub>2</sub> phase might have easily spalled and it might not have worked as a solid lubricant efficiently during the friction tests. The friction coefficients of specimen 1F decreased with increasing testing temperature above 473 K, although the friction coefficients were higher than 0.3 at 1073 K.

Fig. 5 shows the wear rates of Al<sub>2</sub>O<sub>3</sub>, Ni–20mass% Cr and NiAl-based composites containing BaF<sub>2</sub>, CaF<sub>2</sub> and SrF<sub>2</sub> and the coupled Al<sub>2</sub>O<sub>3</sub> balls at 873 K. The wear rates of the specimens and the coupled balls that were friction-tested at 873 K for 3.6 ks were calculated as following procedures. The wear depth profiles of each composite specimen were examined using a surface profilometer. A set of equally spaced depth profiles covering the whole wear track area was used to evaluate the volumetric wear [18–20]. The wear volume of Al<sub>2</sub>O<sub>3</sub> removed from the coupled ball was calculated by measuring the diameter of the wear scar formed on the ball with an optical microscope and assuming that the wear scar was perfectly circular and flat in order to simplify the calculations [18,19,21,22]. The wear rates were obtained by dividing the wear volume (mm<sup>3</sup>) by the load (4.9 N) and the total sliding distance (72 m). Wear rates of Al<sub>2</sub>O<sub>3</sub> specimens were notably reduced by adding BaF<sub>2</sub>, CaF<sub>2</sub> and SrF<sub>2</sub>. In particular, the specimen 1A showed the lowest wear rate among the Al<sub>2</sub>O<sub>3</sub>-based composites. As shown in Fig. 3, the microvickers hardness of specimen 1A was much higher than those of the other Al<sub>2</sub>O<sub>3</sub>-based composites at room temperature. Therefore, the microvickers hardness of specimen 1A might be higher than those of the other Al<sub>2</sub>O<sub>3</sub>-based composites at 873 K, by which the specimen 1A might have shown better wear resistance than the other Al<sub>2</sub>O<sub>3</sub>-based composites at this

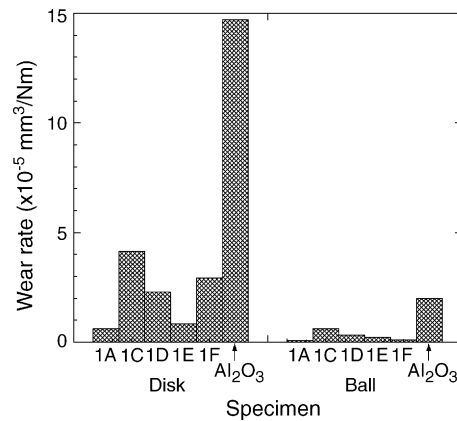


Fig. 5. Wear rates of specimens 1A, 1C, 1D, 1E, 1F and Al<sub>2</sub>O<sub>3</sub> specimens and the coupled Al<sub>2</sub>O<sub>3</sub> balls at 873 K. (Testing time of each specimen was 3.6 ks.)

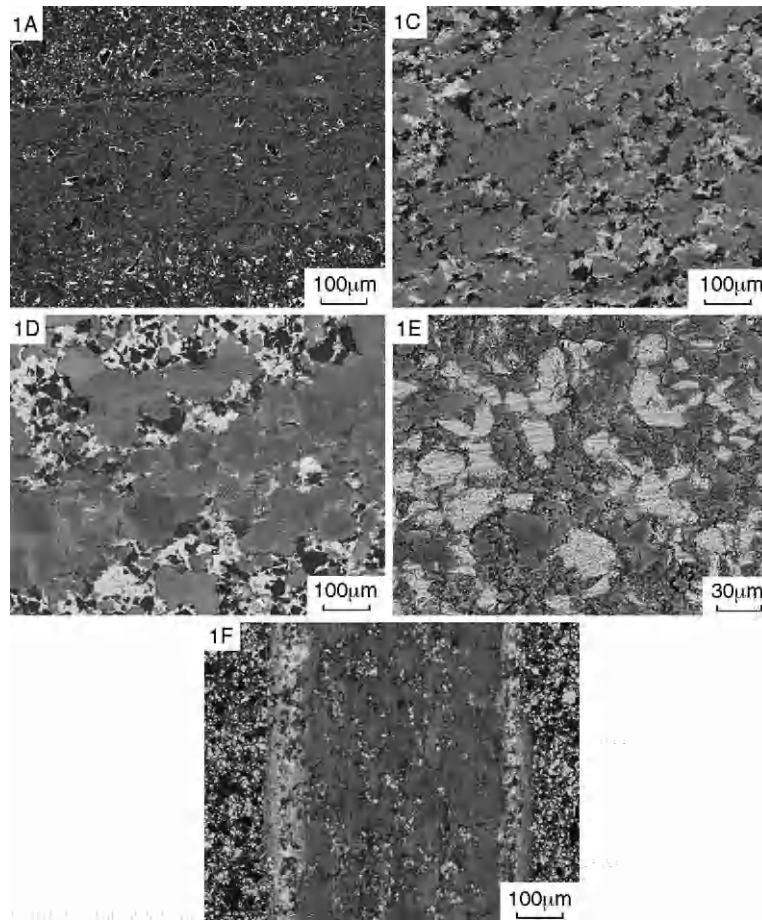


Fig. 6. SEM photographs of worn surface of specimens 1A, 1C, 1D, 1E and 1F after friction testing at 873 K for 3.6 ks.

temperature. In order to confirm these mechanisms, it would be necessary to investigate the mechanical properties of all the  $\text{Al}_2\text{O}_3$ -based composites at high temperatures. Ni–Cr alloy-based and NiAl-based composites containing  $\text{BaF}_2$ – $\text{CaF}_2$  eutectic (specimens 1C and 1D) showed much higher wear rates than the specimen 1A. According to Fig. 3, the microvickers hardness of the specimens 1C and 1D would be much lower than that of the specimen 1A at 873 K, which might have some influence on their wear behaviour. In order to clarify the difference of the wear behaviour of specimens 1A, 1C and 1D, it would be also necessary to investigate their mechanical properties at high temperatures.

Fig. 6 shows the worn surface of specimens 1A, C–F after friction testing at 873 K for 3.6 ks. All the worn surface of the specimens after sliding at 873 K was smooth. According to the EDS analysis, the worn surface of each specimen exhibited the composition similarly to its original surface. The worn surface of  $\text{Al}_2\text{O}_3$  balls after sliding against specimens 1C and 1D at 873 K was covered with Ni–Cr and NiAl alloys films containing a small amount of  $\text{BaF}_2$  and  $\text{CaF}_2$ , respectively. The worn surface of  $\text{Al}_2\text{O}_3$  balls after sliding against  $\text{Al}_2\text{O}_3$ -based composites was partially covered with the films whose compositions were similar to those of the composites. Ouyang et al. reported that  $\text{CaF}_2$  phase in  $\text{Y}_2\text{O}_3$ -

stabilized  $\text{ZrO}_2$ –20 mass%  $\text{CaF}_2$  composite films prepared by low-pressure plasma spraying (LPPS) worked as a solid lubricant above 873 K, and that the worn surface of the composites and the  $\text{Al}_2\text{O}_3$  balls after sliding at 873 and 1073 K were covered with  $\text{CaF}_2$ -matrix film according to the EDS analysis [4,5]. The relative density of composite films prepared by LPPS is normally much lower than that of com-

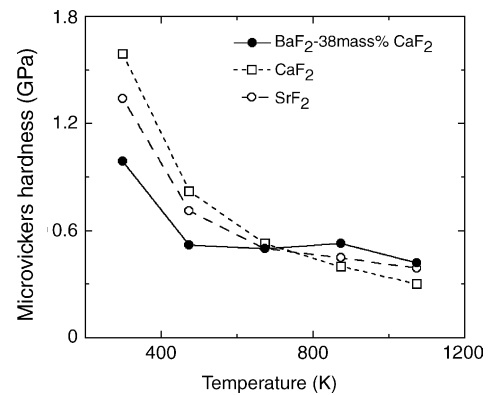


Fig. 7. High-temperature microvickers hardness of  $\text{BaF}_2$ –38 mass%  $\text{CaF}_2$ ,  $\text{CaF}_2$  and  $\text{SrF}_2$  specimens. They were prepared by SPS at 1123, 1573 and 1523 K under a sintering pressure of 40 MPa for 0.3 ks, respectively.

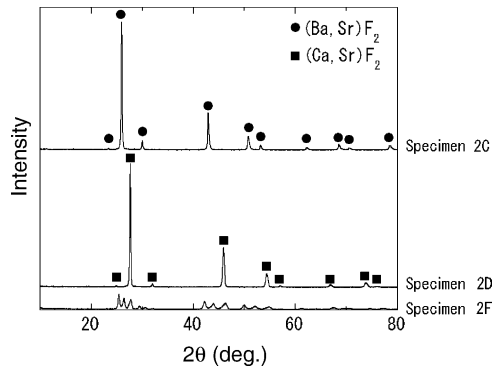


Fig. 8. X-ray diffraction patterns of specimens 2C, 2D and 2F before annealing at 1473 K for 18 ks in an Ar gas atmosphere.

posites prepared by SPS, which indicates that decreasing the relative density of self-lubricating composites may help the solid lubricants work efficiently. In the near future,  $\text{Al}_2\text{O}_3$ -based composites that have various relative densities will be prepared by SPS, and their friction and wear properties will be investigated. In addition, the friction and wear properties of spark-plasma-sintered  $\text{Al}_2\text{O}_3$ -based composites that have various volume fractions of solid lubricant phases will be also examined.

Fig. 7 shows the high-temperature microvickers hardness of  $\text{BaF}_2$ -38 mass%  $\text{CaF}_2$ ,  $\text{CaF}_2$  and  $\text{SrF}_2$  specimens prepared by SPS at 1123, 1573 and 1523 K under a sintering pressure of 40 MPa for 0.3 ks, respectively. All the hardness was measured with a 9.8 N load in an Ar gas atmosphere. It was clarified that their hardness reduced significantly at 473 K.

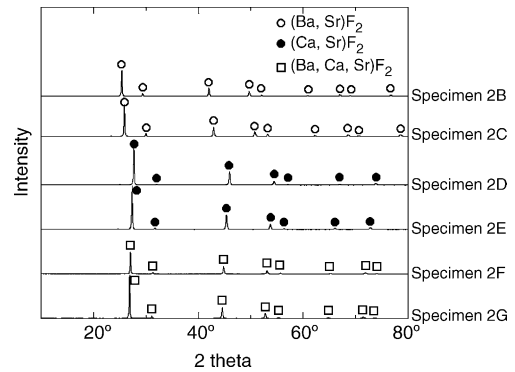


Fig. 9. X-ray diffraction patterns of the specimens of the  $\text{BaF}_2$ - $\text{CaF}_2$ - $\text{SrF}_2$  ternary system after annealing at 1473 K for 18 ks in an Ar gas atmosphere.

Although this softening is expected to have an influence on their friction properties, no clear effects can be observed at around 473 K in Fig. 4. More work will be also needed in order to clarify the effects.

### 3.2. Ternary phase diagram of the $\text{BaF}_2$ - $\text{CaF}_2$ - $\text{SrF}_2$ system

Fig. 8 shows X-ray diffraction patterns of spark-plasma-sintered specimens of the  $\text{BaF}_2$ - $\text{CaF}_2$ - $\text{SrF}_2$  ternary system. Some specimens mainly consisted of single solid phase. However, the other specimens were composed of several phases according to the XRD analysis and SEM observation. This phenomenon would be caused by sluggish diffusion of Ba, Ca and Sr atoms in the specimens. Therefore, all of the

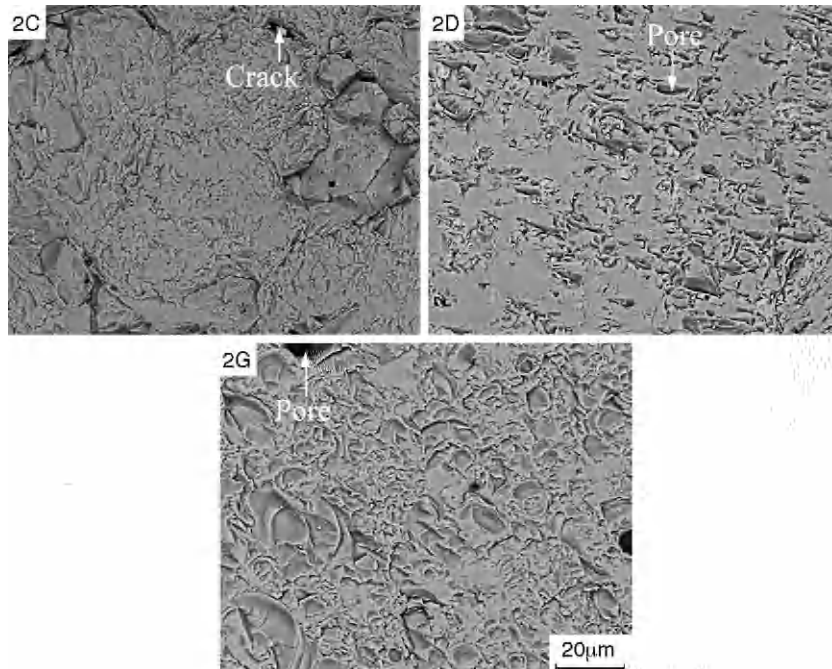


Fig. 10. SEM photographs showing cross sections of the specimens 2C, 2D and 2G after annealing at 1473 K for 18 ks in an Ar gas atmosphere. All of the specimens consisted of one phase, although their microstructure seems to consist of several phases. There are many holes and cleavage planes on the surface of these specimens.

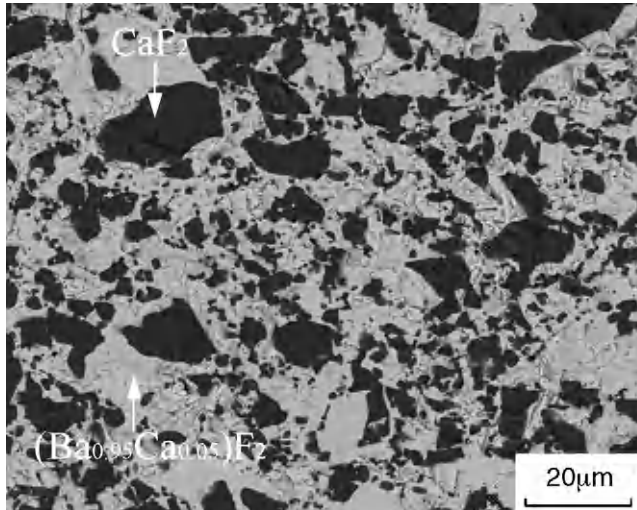


Fig. 11. SEM photograph showing a cross section of specimen 2A before annealing at 1473 K.

specimens as shown in Table 3 were annealed at 1473 K for 18 ks in an Ar gas atmosphere. Fig. 9 shows X-ray diffraction patterns of the specimens after the heat treatment. All of the specimens except for the specimen 2A consisted of single solid phase, which indicates that there is a large solid solution region in the  $\text{BaF}_2\text{--CaF}_2\text{--SrF}_2$  ternary system.

Fig. 10 shows cross sections of some specimens of the  $\text{BaF}_2\text{--CaF}_2\text{--SrF}_2$  ternary system after annealing at 1473 K for 18 ks. All of the specimens except for the specimen 2A consisted of single solid phase, although they contained a large amount of pores. The specimen 2A melted at 1473 K, because the eutectic reaction of the  $\text{BaF}_2\text{--CaF}_2$  system is 1295 K [16]. Fig. 11 shows a cross section of specimen 2A before annealing at 1473 K. The specimen consisted of  $\text{BaF}_2$  and  $\text{CaF}_2$  phases, although the  $\text{BaF}_2$  phase contained a small amount of Ca. This indicates that a small amount of Ca is solid-soluble to  $\text{BaF}_2$ . On the other hand, Ba is hardly solid-soluble to  $\text{CaF}_2$ . Fig. 12 shows a tentative phase diagram of the  $\text{BaF}_2\text{--CaF}_2\text{--SrF}_2$  ternary system. Both the  $\text{BaF}_2\text{--SrF}_2$

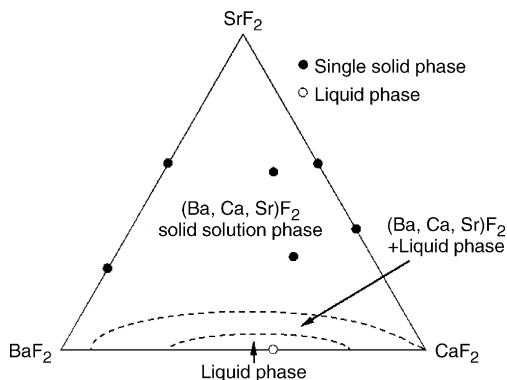


Fig. 12. A tentative  $\text{BaF}_2\text{--CaF}_2\text{--SrF}_2$  ternary phase diagram obtained by examining X-ray diffraction patterns and the microstructure of specimens with seven different compositions annealed at 1473 K for 18 ks in an Ar gas atmosphere.

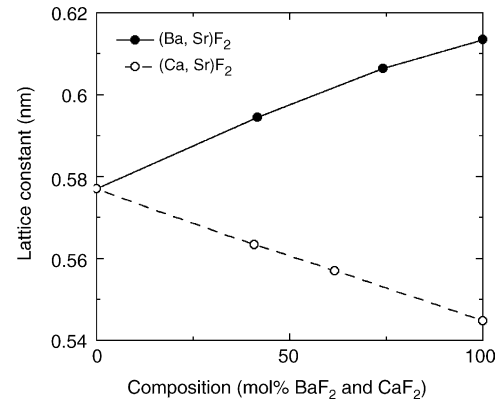


Fig. 13. Lattice constants of specimens of the  $\text{BaF}_2\text{--SrF}_2$  and  $\text{CaF}_2\text{--SrF}_2$  systems obtained in this study.

and  $\text{CaF}_2\text{--SrF}_2$  binary systems were complete solid solution systems, which was consistent with the results reported by Bukhalova et al. and Mateiko et al. [23–26]. Therefore, different types of reaction from the  $\text{BaF}_2\text{--CaF}_2$  system are expected to take place in the  $\text{BaF}_2\text{--SrF}_2$  and  $\text{CaF}_2\text{--SrF}_2$  binary systems, although  $\text{BaF}_2$ ,  $\text{CaF}_2$  and  $\text{SrF}_2$  show the same crystal structure. According to the results obtained in this study, the lattice constants of  $\text{BaF}_2$ ,  $\text{CaF}_2$  and  $\text{SrF}_2$  were 0.6135 nm, 0.5447 nm and 0.5770 nm, respectively. This indicates that both the difference between the lattice constant of  $\text{BaF}_2$  and that of  $\text{SrF}_2$  ( $3.65 \times 10^{-2}$  nm) and the difference between the lattice constant of  $\text{CaF}_2$  and that of  $\text{SrF}_2$  ( $3.23 \times 10^{-2}$  nm) are much smaller than the difference between the lattice constant of  $\text{BaF}_2$  and that of  $\text{CaF}_2$  ( $6.88 \times 10^{-2}$  nm). It is generally known that the A–B binary system exhibits a complete solid solution system, when compounds A and B show the same crystal structure and the difference of their lattice constants is relatively small. Therefore,  $\text{BaF}_2\text{--SrF}_2$  and  $\text{CaF}_2\text{--SrF}_2$  binary systems would have become complete solid solution systems.

Fig. 13 shows the lattice constants of specimens of  $\text{BaF}_2\text{--SrF}_2$  and  $\text{CaF}_2\text{--SrF}_2$  systems. It was clarified that the lattice constants of  $(\text{Ba}, \text{Sr})\text{F}_2$  and  $(\text{Ca}, \text{Sr})\text{F}_2$  linearly increased and decreased with increasing  $\text{BaF}_2$  and  $\text{CaF}_2$  contents, respectively. These tendencies are expected to follow Vegard's law.

As described above, it was shown that the  $\text{BaF}_2\text{--CaF}_2\text{--SrF}_2$  ternary system has a large solid solution region. In the near future, specimens with some different compositions of the  $\text{BaF}_2\text{--CaF}_2\text{--SrF}_2$  ternary system will be prepared by SPS, and their friction properties will be investigated.

#### 4. Conclusions

$\text{Al}_2\text{O}_3$ , Ni–20 mass% Cr, NiAl-based composites containing  $\text{BaF}_2$ ,  $\text{CaF}_2$  and  $\text{SrF}_2$  as solid lubricants were prepared by spark plasma sintering, and their microstructure and high-

temperature friction and wear properties were examined. In addition, a tentative BaF<sub>2</sub>–CaF<sub>2</sub>–SrF<sub>2</sub> ternary phase diagram was constructed. The following conclusions were obtained.

1. Al<sub>2</sub>O<sub>3</sub>–31BaF<sub>2</sub>–19CaF<sub>2</sub> (mass%) composites prepared by spark plasma sintering at 1273 K contained a fine lamellar structure. The lamellar structure consisted of BaF<sub>2</sub> and CaF<sub>2</sub> phases.
2. Using spark plasma sintering, dense Al<sub>2</sub>O<sub>3</sub>, Ni–20 mass% Cr, NiAl-based composites containing BaF<sub>2</sub>, CaF<sub>2</sub> and SrF<sub>2</sub> could be obtained.
3. Al<sub>2</sub>O<sub>3</sub>–31BaF<sub>2</sub>–19CaF<sub>2</sub> (mass%) composites showed the lowest friction coefficient at temperatures between room temperature and 1073 K, and showed the lowest wear rate at 873 K.
4. Microvickers hardness of BaF<sub>2</sub>–38 mass% CaF<sub>2</sub>, CaF<sub>2</sub> and SrF<sub>2</sub> specimens was notably reduced above 473 K.
5. The BaF<sub>2</sub>–CaF<sub>2</sub>–SrF<sub>2</sub> ternary system has a large solid solution region at 1473 K.

### Acknowledgements

This study was supported as R&D on an Environmentally Compatible Propulsion System for Next-Generation Supersonic Transport (ESPR)”, an Industrial Technology Program of the New Energy and Industrial Technology Development Organization (NEDO) of Japan.

### References

- [1] H.E. Sliney, J.W. Graham, J. Lubr. Technol., Trans. ASME, Series F 97 (1975) 506.
- [2] H.E. Sliney, ASLE Trans. 29 (1985) 370.
- [3] Y. Jin, K. Kato, N. Umehara, Tribol. Lett. 4 (1998) 243.
- [4] J.H. Ouyang, S. Sasaki, K. Umeda, Surf. Coat. Technol. 137 (2001) 21.
- [5] J.H. Ouyang, S. Sasaki, K. Umeda, Wear 249 (2001) 440.
- [6] K. Umeda, S. Takatsu, A. Tanaka, Abstracts of papers of World Tribol. Congress, IMechE 1997, p. 686.
- [7] K. Umeda, A. Tanaka, S. Takatsu, in: Proceeding of the International Tribology Confress, Japanese Society of Tribologists, Nagasaki 2000, p. 1161.
- [8] J.H. Ouyang, S. Sasaki, K. Umeda, Surf. Coat. Technol. 154 (2002) 131.
- [9] T. Murakami, J.H. Ouyang, A. Korenaga, K. Umeda, S. Sasaki, Y. Yoneyama. Mater. Trans., in press.
- [10] M. Tokita, J. Soc. Powder Technol. (Jpn.) 30 (1993) 790.
- [11] T. Murakami, S. Sasaki, K. Ito, H. Inui, M. Yamaguchi, Intermetallics 12 (2004) 749.
- [12] T. Murakami, S. Sasaki, K. Ito, Intermetallics 11 (2003) 269.
- [13] T. Murakami, S. Sasaki, K. Ichikawa, A. Kitahara, Intermetallics 9 (2001) 629.
- [14] T. Murakami, S. Sasaki, K. Ichikawa, A. Kitahara, Intermetallics 9 (2001) 621.
- [15] H. Kim, M. Kawahara, M. Tokita, J. Jpn. Soc. Powder Metall. 47 (2000) 887.
- [16] G.A. Bukhalova, V.T. Berezhnaya, A.G. Bergman, Zh. Neorgan. Khim. 6 (1961) 2359.
- [17] H.E. Sliney, T.N. Strom, G.P. Allen, ASLE Trans. 8 (1965) 307.
- [18] J.H. Ouyang, S. Sasaki, Surf. Coat. Technol. 187 (2004) 343.
- [19] J.H. Ouyang, S. Sasaki, T. Murakami, K. Umeda, Mater. Sci. Eng. A386 (2004) 234.
- [20] M.Z. Huq, J.P. Celis, Wear 225–229 (1999) 53.
- [21] M. Shuaib, T.J. Davies, Wear 249 (2001) 20.
- [22] A.W. Ruff, ASM Handbook, Friction, Lubrication and Wear Technology, vol. 18, 1990, p. 363.
- [23] G.A. Bukhalova, Z.A. Mateiko, V.T. Berezhnaya, Zh. Neorgan. Knim. 7 (1962) 1655.
- [24] G.A. Bukhalova, V.T. Berezhnaya, Z.A. Mateiko, Zh. Neorgan. Knim. 7 (1962) 2233.
- [25] Z.A. Mateiko, G.A. Bukhalova, Zh. Neorgan. Knim. 7 (1962) 165.
- [26] Z.A. Mateiko, G.A. Bukhalova, Zh. Neorgan. Knim. 6 (1961) 882.